Available online at www.sciencedirect.com
SCIENCE DIRECT
Journal of Catalysis 232 (2005) 108–116
JOURNAL OF CATALYSIS
www.elsevier.com/locate/jcat

Characterization and hydroformylation performance of mesoporous MCM-41-supported water-soluble Rh complex dissolved in ionic liquids

Yong Yang, Changxi Deng, Youzhu Yuan *

State Key Laboratory for Physical Chemistry of Solid Surfaces, Department of Chemistry, Xiamen University, Xiamen 361005, China

Received 26 January 2005; revised 15 February 2005; accepted 18 February 2005

Available online 7 April 2005

Abstract

The TPPTS-Rh complex [TPPTS = trisodium salt of tri-(*m*-sulfophenyl)-phosphine, $P(m\text{-}C_6H_4SO_3Na)_3$], which was dissolved in the ionic liquids 1-butyl-3-methyl-imidazolium tetrafluoroborate ($BMI{\cdot}BF_4$), 1-butyl-3-methyl-imidazolium hexafluorophosphate ($BMI{\cdot}PF_6$), and 1,1,3,3-tetramethylguanidinium lactate (TMGL), was immobilized on MCM-41. The resulting supported ionic liquid-phase catalysts (SILPCs) were very active for the hydroformylation of higher olefins. The SILPCs with the regular hexagonal array of MCM-41 were structurally stable before and after the catalytic reaction, as characterized by XRD, N_2 adsorption/desorption, FTIR, ^{31}P-NMR, SEM, HRTEM, and TGA-DSC. The obtained SILPCs showed higher catalytic activity, independent of IL type, as compared with their ionic liquid–organic biphasic counterparts and the one with SiO_2 as carrier. Such SILPCs could be reused several times without significant loss of activity or selectivity.

Keywords: MCM-41; Ionic liquid; Supported ionic liquid catalyst (SILPC); Water-soluble rhodium complex; Hydroformylation; Higher olefin

1. Introduction

Ionic liquids (ILs) exhibit many favorable features compared with conventional molecular solvents, such as low vapor pressure and wide liquid temperature range, which, in combination with their ability to dissolve a wide range of organics and organometallics and even some inorganic compounds, makes them versatile engineering solvents [1–4]. Much attention has been focused in recent years on the ILs as alternative reaction media. In particular, based on their highly charged nature, the IL phases are ideal for biphasic reactions in organic synthesis and catalysis [5–16]. A number of works have described the improvements obtained through the substitution of water or organic solvent, with the ILs as solvent, for immobilization of organometallic catalysts, resulting in improved catalytic performance and easy catalyst–product separation [17–21]. For instance, in the rhodium-catalyzed hydroformylation of olefins, Chauvin et al. have pointed out that the $Rh(CO)_2(acac)/PPh_3$ system in ILs such as $BMI{\cdot}PF_6$ and $BMI{\cdot}BF_4$ showed good catalytic performance in the hydroformylation of 1-pentene, although part of the active rhodium catalyst was extracted into the organic phase [22]. Polar ligands such as trisodium salt of tri-(*m*-sulfophenyl)-phosphine [TPPTS, $P(m\text{-}C_6H_4SO_3Na)_3$] and monosulfonated triphenylphosphine [TPPMS, $P(C_6H_5)_2(m\text{-}C_6H_4SO_3Na)$] were used to modify the uncharged $Rh(CO)_2(acac)$ in the ILs for olefin hydroformylation. Favre et al. found that the problem of Rh leaching could be minimized by the modification of phosphorus ligands with cationic (guanidinium or pyridinium) or anionic (sulfonate) groups [23].

However, a reduction of the amount of IL in the reaction processes and the introduction of cheap, halogen-free, and easily prepared ILs as new, greener solvents are desirable from the economic and toxicological points of view. The concept of supported IL-phase catalysts (SILPCs) is one of the smart techniques for IL chemistry. Such SILPCs have been applied in alkylation, olefin hydroformylation,

* Corresponding author. Fax: +86-592-2183047.
E-mail address: yzyuan@xmu.edu.cn (Y. Yuan).

0021-9517/$ – see front matter
doi:10.1016/j.jcat.2005.02.017

hydrogenation, the Heck reaction, and hydroamination [24–35]. Mehnert et al. have reported the creation of a SILPC through the immobilization of homogeneous Rh complexes in ILs on SiO_2 [25,26,32]. They found that such a SILPC system showed rather good performance in hydrogenation and hydroformylation with respect to IL-organic biphasic catalysis. Riisager et al. found that it is possible to use SiO_2-supported IL-phase Rh-phosphine catalysts for hydroformylation of propene and 1-octene in a fixed-bed reactor and that a specially designed water-soluble bidentate phosphine ligand was required to obtain a better aldehyde n/i ratio and higher catalytic stability [27,28,34].

Mesoporous molecular sieves synthesized with the aid of micelle templates have shown huge surface areas, well-ordered periodic structures, and controllable pore size when the template molecule has been varied and/or additives such as trimethylbenzene have been used [35]. These characteristics of mesoporous molecular sieves are potential attractive features of novel catalysts for chemical reactions. Nanopores in particular have been explored as a site for the confinement of various materials and their reactions, which could lead to many practical applications, ranging from catalysis to conducting materials [36]. The ability to control the pore size, channel connectivity, and morphology opens up the possibility of using these materials as nanoreactors in which chemical processes can be tailor-designed for detailed studies. However, the range of application has been limited by the instability of the structure of mesoporous molecular sieves like MCM-41. MCM-41 has been reported to have high thermal stability and hydrothermal stability in air and oxygen-containing water vapor, but it has low hydrothermal stability in water and aqueous solutions. It has been observed to lose its original structure during heating in boiling water and aqueous solutions [37–39]. To date, information on the structure and catalysis of SILPCs based on ordered mesoporous silicas like MCM-41 has been scarce in the literature.

Recently we reported that a higher performance of 1-hexene hydroformylation could be achieved with the mesoporous MCM-41 supported water-soluble TPPTS-Rh complex dissolved in the IL TMGL as a novel and robust heterogeneous catalyst [40]. The present study reports the structural features of the water-soluble Rh-TPPTS complex in the ILs TMGL, BMI·BF_4, and BMI·PF_6 at the surface of MCM-41 and its catalytic performance in the hydroformylation of higher olefins, as observed by means of XRD, N_2 adsorption/desorption, TGA-DSC, FTIR, ^{31}P-NMR, SEM, and HRTEM.

2. Experimental

2.1. General comments

All experiments were performed under an atmosphere of dry argon with standard Schlenk techniques. TPPTS and ILs TMGL, BMI·PF_6, and BMI·BF_4 were prepared according to procedures described in the literature [41–43] and dried in vacuum before use. The MCM-41 and SiO_2 (200 mesh) were dehydrated under vacuum at 523 K for 3 h in a Schlenk tube. Methanol was dried over 3-Å molecular sieves and distilled before use. Toluene was dried with $CaCl_2$ and Na pieces. 1-Hexene was purchased from Aldrich and used without further purification.

2.2. Catalyst preparation

Mesoporous MCM-41 was synthesized by procedures described elsewhere [44–46]. In a typical synthesis of SILPC, 10 mg of $Rh(CO)_2(acac)$ (0.038 mmol) and 110 mg of TPPTS (0.19 mmol) were dissolved in 10 ml of degassed dry methanol. After the desired amount of IL was added, the solution was stirred at room temperature under argon for 2 h. The carrier (0.5 g), which was pretreated under vacuum at 523 K for 3 h, was added to the above solution. The mixture was stirred under argon for 2 h. A light yellow SILPC was obtained by removal of solvent under vacuum, followed by drying in vacuum at 353 K for 24 h. The catalyst was stored in argon before use and was designated as IL-TPPTS-Rh/MCM-41. For example, the sample of 15 wt% TMGL-TPPTS-Rh/MCM-41 had a TMGL loading of 15 wt% based on the pure MCM-41 silicate.

2.3. Characterization

The SILPCs were characterized by FT-IR, liquid-state ^{31}P NMR, XRD, N_2 adsorption/desorption, SEM, HRTEM, and TGA-DSC. The FT-IR spectra were measured on a Nicolet 740 spectrometer in KBr pellets at a resolution of 4 cm^{-1}. The powder XRD patterns were recorded at room temperature on an X'Pert PRO X-ray diffractometer with Cu-K_α radiation at 40 kV and 30 mA. The 2θ angles were scanned from 1.5° to 10° at a rate of 1°/min. The properties of the porous structures were determined from N_2 adsorption/desorption measurements at 77 K with a Micromeritics ASAP 2010M + C system. The sample was outgassed under vacuum at 403 K for 3 h before the adsorption of nitrogen. The BJH method, based on the Kelvin equation, was applied to evaluate the mesopore size distribution from the adsorption branch. We standardized the total pore volume for all samples against the weight of pure mesoporous silicas by subtracting the weight of the ionic liquid and TPPTS-Rh complex. The microporous volume was evaluated by the t-plot method. SEM images were taken with a LEO 1530 electron probe X-ray microanalyzer. For the SEM observations, the samples were deposited on a sample holder and coated with Au. High-resolution TEM (HRTEM) images were obtained on a Philips TECNAI F-30 FEG instrument at an accelerating voltage of 300 kV. The sample was dispersed with dry ethanol. The TGA-DSC profiles were recorded on a NETZSCH STA 449 C analyzer with Al_2O_3 as a reference. The measurements were carried out with a dynamic temperature program of 298–1073 K at a heating rate 10 K/min in

air. The rhodium leaching content was detected by atomic adsorption spectroscopy (AAS) on a WFX-1E2 instrument. The reaction products were condensed and dissolved with HNO_3. ^{31}P-NMR spectroscopy was recorded on a Varian FT Unity$^+$ 500 spectrometer at 202 MHz at room temperature in DMSO-d_6. The chemical shift was referenced to 85% H_3PO_4.

2.4. Hydroformylation

Typical olefin hydroformylation was carried out in a 100-ml stainless-steel autoclave with a mechanical stirrer. After the introduction of the required amount of catalyst, olefin and toluene were placed in the autoclave. The reactor was then pressurized three times with 1.0 MPa of CO/H_2 (1:1 volume ratio). Then the autoclave was pressurized with the same gas mixture at the desired pressure and heated to the reaction temperature. After reaction, the reactor was cooled with an ice bath and decompressed. The oils and the catalysts were separated by centrifugation. The organic phase was analyzed with a gas chromatograph equipped with FID and a capillary column (SE-30, 30 m × 0.32 mm × 0.25 μm).

3. Results and discussion

3.1. Characterization by XRD and N_2 adsorption/desorption

The Rh precursor $Rh(CO)_2(acac)$ was readily dissolved in the ILs TMGL, BMI·BF_4, and BMI·PF_6. The TPPTS ligand, however, showed very low solubility in those ILs. Thus the small amount of TPPTS was dissolved in methanol with stirring. A pale yellow homogeneous solution containing the methanol, IL, TPPTS, and Rh precursor could be obtained. The MCM-41-SILPC was then prepared after the conventional impregnation and vacuum removal of methanol. Fig. 1 shows the XRD patterns of the as-synthesized MCM-41 and the MCM-41-SILPCs with different TMGL loadings. All samples exhibited the typical low-angle *hkl* reflections characteristic of the 2D hexagonal *P6mm* structure. The overall mesoporous hexagonal structure in the SILPCs was maintained, although loss of the peak intensities in the XRD pattern was observed as the TMGL loading was increased. The peaks at higher degree (d_{210}) almost disappeared for the samples after immobilization of the TMGL-TPPTS-Rh complex, especially for TMGL loadings higher than 25 wt%.

Evidence that there were no significant differences in the XRD patterns and N_2 adsorption/desorption isotherms for the SILPC before and after heat treatment in toluene at 373 K for 100 h indicated that the SILPC derived from the ordered mesoporous MCM-41 was structurally stable. N_2 adsorption/desorption isotherms for the as-prepared SILPCs with different TMGL loadings are shown in Fig. 2. The shape of the isotherm remained unchanged compared with that of MCM-41. The inflection point of the capillary condensation,

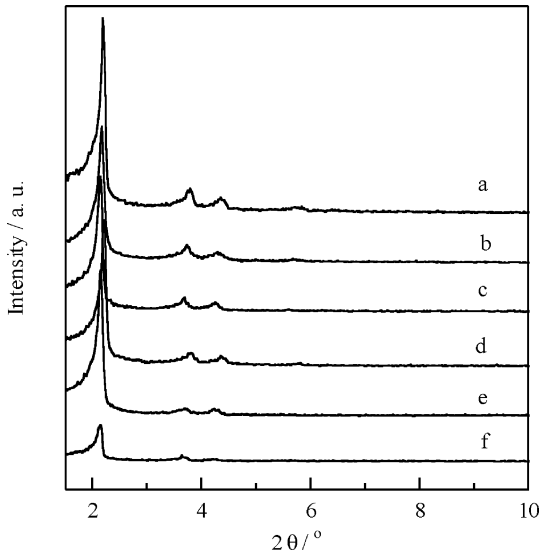

Fig. 1. The XRD patterns for the TMGL-TPPTS-Rh/MCM-41 SILPCs. The TMGL loadings are (wt%): (a) 0; (b) 5; (c) 10; (d) 15; (e) 25; (f) 50.

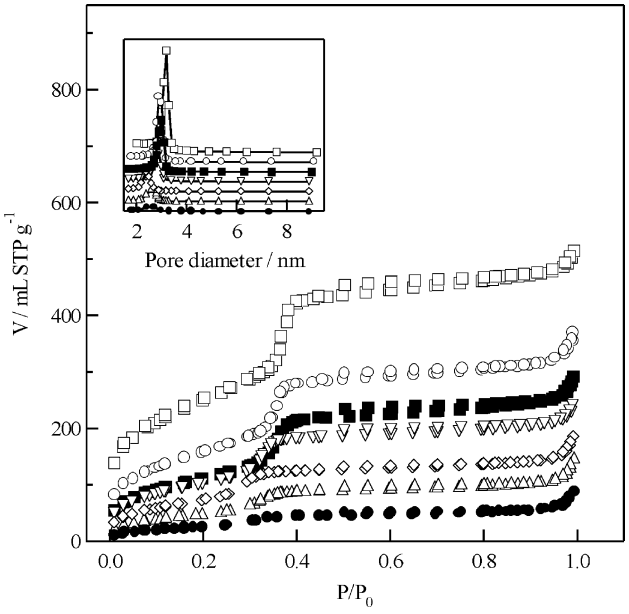

Fig. 2. The N_2 adsorption isotherms and the pore size distributions for MCM-41 and the TMGL-TPPTS-Rh/MCM-41 SILPCs. (□) MCM-41; the SILPC with TMGL loadings at (wt%): (○) 0; (■) 5; (▽) 10; (◇) 15; (△) 25; (●) 50.

however, became less sharp and shifted to lower relative pressures. The pore size distribution based on the Kelvin relation is also shown in Fig. 2 (inset). The results show that the amount of physisorbed nitrogen decreased with an increase in the TMGL loading, causing a reduction in the surface area, total pore volume, and mean pore size, as listed in Table 1. For comparison, the d_{100} values, the hexagonal unit cell parameter (α_0), and the size of the silicate wall (s) are incorporated into Table 1. The d_{100} reflection peak for the SILPC samples shifted slightly to higher 2θ (degree) values compared with that of MCM-41. The d spacing of

Table 1
The textural property and pore structure of the MCM-41-SILPC and relevant samples

Catalyst	ILs loading		S_{BET}[b] ($m^2\ g^{-1}$)	$V_{p\ tot}$[c] ($cm^3\ g^{-1}$)	V_{μ}[d] ($cm^3\ g^{-1}$)	d_{100}[e] (nm)	α_0[f] (nm)	d_{BJH}[g] (nm)	s[h] (nm)
	wt%	α[a]							
MCM-41	0	–	1041	0.789	0	4.06	4.68	3.0	1.68
TPPTS-Rh/MCM-41	0	0	990	0.586	0	4.09	4.72	2.8	1.92
TMGL-TPPTS-Rh/MCM-41	5	0.038	574	0.493	0	4.15	4.79	2.7	2.09
	10	0.079	469	0.385	0	4.13	4.77	2.5	2.27
	15	0.126	402	0.344	0	4.12	4.76	2.6	2.16
	25	0.237	250	0.233	0	4.11	4.75	2.3	2.45
	50	0.711	153	0.173	0	4.11	4.75	2.1	2.65
BMI·PF_6-TPPTS-Rh/MCM-41	5	0.029	623	0.473	0	4.08	4.71	2.8	1.91
	10	0.062	571	0.389	0	4.14	4.78	2.8	1.97
	15	0.098	493	0.224	0	4.17	4.77	2.6	2.17
	25	0.185	257	0.161	0	4.10	4.74	2.6	2.08
	50	0.555	243	0.103	0	4.17	4.82	2.2	2.62
BMI·BF_4-TPPTS-Rh/MCM-41	10	0.072	316	0.338	0	4.09	4.73	2.9	1.83

[a] Pore filling degrees of ionic liquids in the MCM-41 support as volume IL/pore volume support.
[b] BET specific surface area.
[c] Total pore volume.
[d] Micropore volume.
[e] XRD (100) interplaner spacing.
[f] Hexagonal unit cell parameter, $\alpha_0 = 2d_{100}/\sqrt{3}$.
[g] Mean pore diameter determined by BJH method.
[h] Size of silicate wall.

the samples increased with the increasing IL loading. With the unit cell parameter (α_0) and mean pore size (d_{BJH}) reported in Table 1 taken into consideration, it was possible to calculate the size of the silica walls (s) around the hexagonal arrangement of the cylindrical pores with the equation $\alpha_0 = d_{BJH} + s$. The increasing size of the silica walls might be correlated with the decrease in the order, as observed in the XRD patterns. The decreases in peak intensities and the increase in the size of the silica walls are possibly related to the amount of IL-TPPTS-Rh complex located in the inner channels of MCM-41. As more IL-TPPTS-Rh complex was immobilized, the Bragg reflections became less intense.

A careful t-analysis, with a nonporous silica isotherm reported in the literature as a reference [47,48], is shown in Fig. 3. For MCM-41 and the SILPCs, upward deviations were observed for pore sizes larger than 2.3 nm. The upward deviations indicate the presence of capillary condensation in mesopores and exclude the presence of micropores in any of the samples. Therefore, the reduction in surface area, pore volume, and pore size could be attributed to the fact that the IL-TPPTS-Rh complex is essentially dispersed at the inner walls of the mesopores.

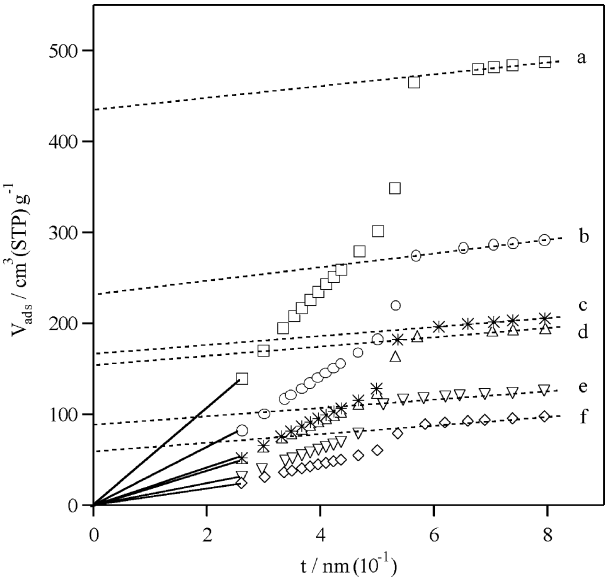

Fig. 3. The nitrogen t-plot curves for MCM-41 and the TMGL-TPPTS-Rh/MCM-41 SILPCs. (a) MCM-41; the SILPC with TMGL loadings at (wt%): (b) 0; (c) 5; (d) 10; (e) 15; (f) 25.

3.2. SEM and HRTEM characterization

The SEM images for MCM-41 and the SILPC with a TMGL loading of 15 wt% are shown in Figs. 4A and 4B. The morphology of the SILPC was similar to, but smoother than, that of MCM-41. A thin film-like material appeared at the surface of SILPC. Figs. 4C and 4D shows HRTEM images for MCM-41 after heating in TMGL at 373 K for 100 h and for the as-prepared SILPC with 15 wt% TMGL loading. No dramatic differences could be observed among the images of the as-prepared MCM-41 (not shown), the one after 100 h of heat treatment in the TMGL and the SILPC. The results revealed that the regular hexagonal arrays of MCM-41 remained unchanged with the treatment under different conditions. We have checked the HRTEM images of MCM-41-SILPC derived from BMI·BF_4 and found that this sample also showed typical regular hexagonal arrays for the ordered mesoporous MCM-41.

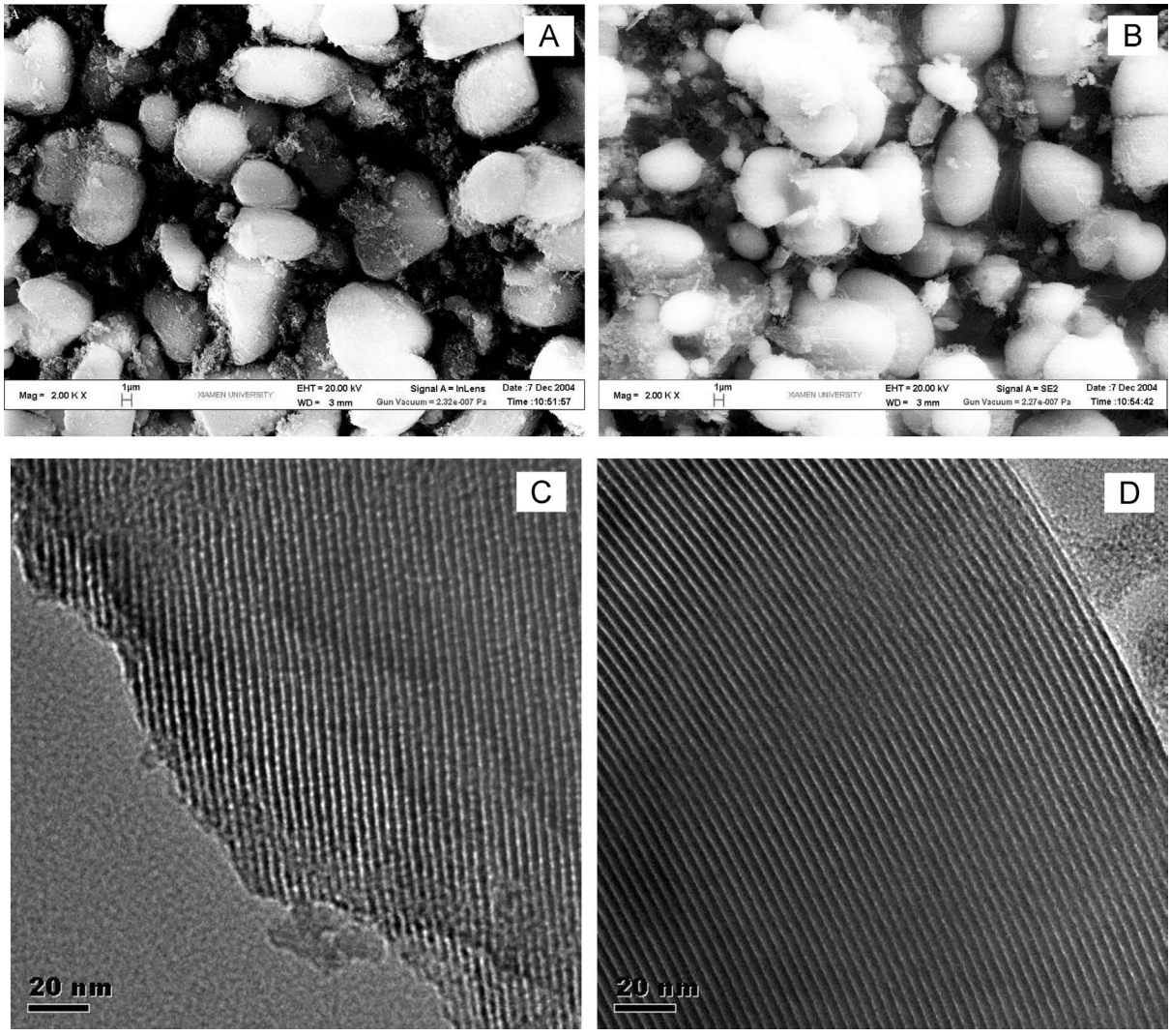

Fig. 4. The SEM and HRTEM images for MCM-41 and the TMGL-TPPTS-Rh/MCM-41 SILPC with 15 wt% of TMGL. (A) The SEM image with magnification of 2000 for MCM-41; (B) The SEM image with magnification of 2000 for the SILPC with 15 wt% of TMGL; (C) The HRTEM image for MCM-41 after heating in the TMGL at 373 K for 100 h; (D) The HRTEM image for the SILPC with 15 wt% of TMGL.

3.3. TGA characterization

Fig. 5 depicts TGA-DSC profiles for TMGL and the SILPCs with TMGL loadings of 5, 10, and 25 wt%. The TGA graph for TMGL showed a continuous weight loss from about 350 K. There was a very small DSC peak at about 373–393 K, corresponding to a $\sim$ 4% weight loss. The weight loss might be attributed to the vaporization of adsorbed water. A large endothermic peak at 500 K apparently corresponded to the major decomposition of TMGL. The SILPC samples before and after the catalytic run (curves Fig. 5b–c) also showed TGA-DSC responses at 373–393 K and 500 K similar to that of TMGL. The weight losses at 500 K were in good agreement with the loadings of TMGL. However, a sharp endothermic peak at 690 K, which might be ascribed to the structural decomposition of TPPTS-Rh complexes, was observed for the SILPC samples, as indicated by the TGA-DSC profiles for the pure complexes of $Rh(CO)Cl(TPPTS)_2$ and $HRh(CO)(TPPTS)_3$ (curves f and g, Fig. 5). Fig. 5a also shows that the complexation between TPPTS and $Rh(CO)_2(acac)$ was not complete in the absence of TMGL. In other words, the presence of TMGL might be necessary for the complexation between TPPTS and Rh species during catalyst preparation.

3.4. Characterization by FT-IR and ^{31}P-NMR

Fig. 6 shows FT-IR spectra for the various SILPCs and relevant samples. The MCM-41-supported $Rh(CO)_2(acac)$ in TMGL gave two carbonyl stretching frequencies at 2080 and 2010 cm^{-1} (curve c), which were due to the contribution of the precursor $Rh(CO)_2(acac)$. The as-prepared SILPC with TMGL and TPPTS/Rh = 5 (curve d), however, showed one peak in the CO stretching region at 1984 cm^{-1} but no peaks at 1560 and 1520 cm^{-1} for coordinated *acac*. After the catalytic reaction and when ILs BMI·BF_4 and BMI·PF_6

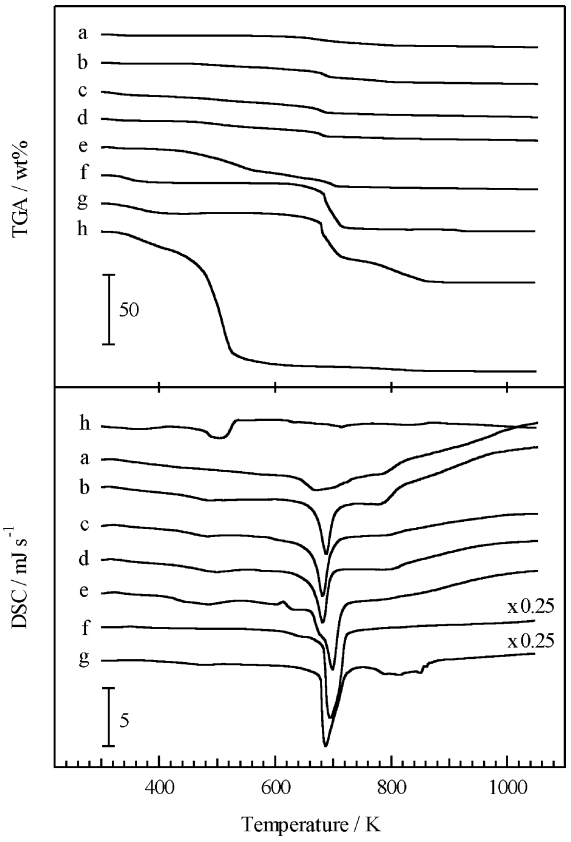

Fig. 5. The TGA-DSC profiles for the TMGL-TPPTS-Rh/MCM-41 SILPCs, TPPTS-Rh complexes and TMGL under air. The SILPC with TMGL loadings at (wt%): (a) 0; (b) 5; (c) sample (b) after the 1-hexene hydroformylation at 373 K; (d) 10; (e) 25; (f) $RhCl(CO)(TPPTS)_2$; (g) $HRh(CO)(TPPTS)_3$; (h) TMGL.

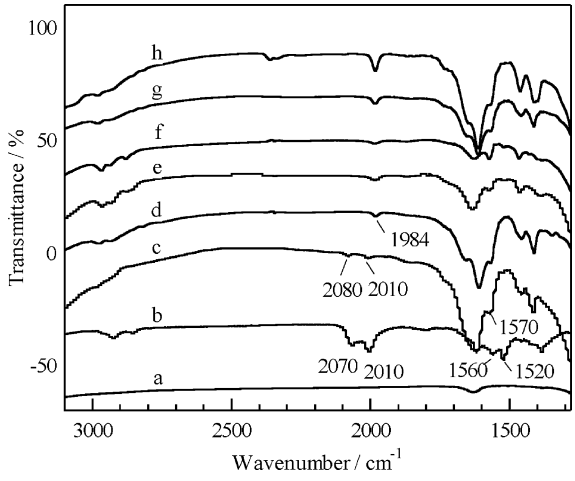

Fig. 6. The FT-IR spectra for MCM-41, $Rh(CO)_2(acac)$ and the MCM-41 -SILPCs. (a) MCM-41; (b) $Rh(CO)_2(acac)$; (c) $Rh(CO)_2(acac)$/MCM-41 with 15 wt% of TMGL; (d) the SILPC with 15 wt% of TMGL and TPPTS/Rh = 5 (molar ratio); (e) the SILPC with 15 wt% of $BMI{\cdot}BF_4$ and TPPTS/Rh = 5 (molar ratio); (f) the SILPC with 15 wt% of $BMI{\cdot}PF_6$ and TPPTS/Rh = 5 (molar ratio); (g) the SILPC with 15 wt% of TMGL and TPPTS/Rh = 5 (molar ratio) after the sixth recycling; (h) the SILPC with 15 wt% of TMGL and TPPTS/Rh = 20 (molar ratio).

were used or the TPPTS/Rh molar ratio was increased, the IR spectra for these SILPCs were identical to those mentioned above, confirming that the same product was formed at the surfaces of MCM-41 and that it was robust.

Fig. 7 shows ^{31}P-NMR spectra for TPPTS-Rh/MCM-41 and several SILPCs. The ^{31}P-NMR spectrum of TPPTS-Rh/MCM-41 in the absence of IL showed three resonance peaks at −4.2, 26.9, and 46.8 ppm (d, $^1J_{Rh-P} = 175$ Hz),

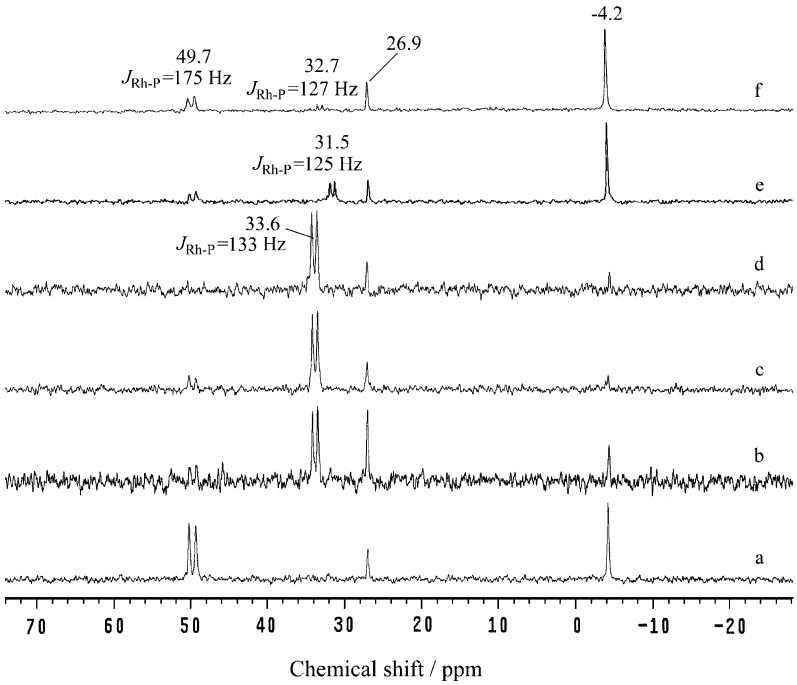

Fig. 7. The ^{31}P-NMR spectra for the MCM-41-SILPCs with TPPTS/Rh = 5 (molar ratio). The TMGL loadings at (wt%): (a) 0; (b) 5; (c) 10; (d) 25; (e) the $BMI{\cdot}BF_4$ loading at 10 wt%; (f) the $BMI{\cdot}PF_6$ loading at 10 wt%.

due to TPPTS, OTPPTS, and Rh(CO)(TPPTS)(*acac*), respectively. As for the SILPC with TMGL, BMI·BF_4, or BMI·PF_6, the ^{31}P-NMR spectra showed a doublet at 31.5–33.6 ppm (d, $^1J_{Rh-P} = 125$–133 Hz) for the rhodium-bound TPPTS ligand and a resonance at 26.1 ppm for the uncoordinated phosphine oxide species tri(*m*-sulfonyl)triphenylphosphine oxide trisodium (TPPTS-oxide) [49]. The intensity of the peak at 46.8 ppm decreased when the peak at 33.6 ppm appeared and with increasing TMGL loadings (curves b, c, and c, Fig. 7). Under the same conditions, the as-prepared SILPCs with BMI·BF_4 and BMI·PF_6 gave a much weaker resonance at 33.6 ppm, implying that the reaction of Rh(CO)$_2$(*acac*) and TPPTS was not accomplished, because of the lower solubility of TPPTS in the ILs [23,49]. The complexation of TPPTS and rhodium species, however, conceivably proceeded under the reaction conditions, as indicated by the ^{31}P-NMR observation that, after the reaction, the SILPCs with BMI·BF_4 or BMI·PF_6 afforded an intensive doublet around 31.5–33.6 (d, $^1J_{Rh-P} = 125$–133 Hz) and 26.9 ppm (not shown).

It is known that Rh(CO)$_2$(*acac*) and phosphines (L) react in a 1:1 ratio and give the complex Rh(CO)L(*acac*). For L = PPh_3 this complex exhibited a doublet at 48.7 ppm with a Rh–P coupling constant of 175 Hz in its ^{31}P-NMR spectrum [50]. *trans*-Rh(CO)(PPh_3)$_2$X complexes (where X is an anion or a solvate molecule) exhibit a doublet in their ^{31}P-NMR spectra around 30 ppm and CO stretching frequencies around 1980 cm^{-1} [51]. Furthermore, reaction of Rh(CO)$_2$(*acac*) with excess TPPTS gave *trans*-Rh(CO)(OH)(TPPTS)$_2$, which exhibited a doublet at 31.8 ppm ($^1J_{Rh-P} = 129$ Hz) [52]. Hence, we deduce that the reaction between Rh(CO)$_2$(*acac*) and TPPTS in the ILs was similar to that in aqueous system. During the preparation of the SILPC, *trans*-Rh(CO)(O–Si≡)(TPPTS)$_2$ was likely formed in the thin IL layer at the MCM-41 surface [53]. Such a species would be active and structurally stable for the olefin hydroformylation in liquid phase.

3.5. Hydroformylation

Table 2 compares the performances in the hydroformylation of higher olefins for the IL-organic biphasic system with and without ligand TPPTS and the SILPC with TMGL. The catalytic activity was not satisfactory and depended on the type of IL in the biphasic catalysts composed of the IL phase and the organic phase. Next, the pale yellow homogeneous solution containing methanol, IL, TPPTS, and the Rh precursor was charged to prepare the MCM-41-SILPC. A much higher catalytic activity was achieved with this catalyst than with the IL-organic biphasic system. The hydroformylation of higher olefins such as 1-octene, 1-decene, and 1-dodecene proceeded under mild conditions.

The catalytic performance over the SILPCs was affected significantly by the IL loading and by the type of carrier. Table 3 shows the 1-hexene conversions and n/i aldehyde ratios versus the TMGL loadings for the SILPCs with MCM-41 and SiO_2 as carriers. The TPPTS/Rh molar ratio was kept at 5. The SILPC using SiO_2 as a carrier afforded a reasonable n/i aldehyde ratio, but gave a lower 1-hexene conversion as compared with the MCM-41-SILPC under identical conditions. The n/i aldehyde ratio increased from 0.7 to 3.5 as the TMGL loading increased from 0 to 25 wt% for the MCM-41-SILPC. A further increase in the TMGL loading caused

Table 2
The olefin hydroformylation catalyzed by IL-organic biphasic system and the MCM-41-SILPC with 5 wt% of TMGL[a]

Catalyst	Substrate	n/i	Conversion (%)	TOF (h^{-1})
TMGL-Rh[b]	1-hexene	3.2	5.0	32
BMI·PF_6-Rh[b]	1-hexene	2.4	3.7	23
BMI·BF_4-Rh[b]	1-hexene	2.2	3.4	22
TMGL-TPPTS-Rh[b]	1-hexene	3.8	13.0	82
BMI·PF_6-TPPTS-Rh[b]	1-hexene	2.5	8.0	50
BMI·BF_4-TPPTS-Rh[b]	1-hexene	2.3	43.4	271
TMGL-TPPTS-Rh/MCM-41	1-hexene	2.7	55.6	348
	1-octene	1.6	39.1	195
	1-decene	1.3	18.0	74
	1-dodecene	1.5	15.2	55

[a] Reaction conditions: TMGL-TPPTS-Rh/MCM-41 = 0.1 g, TMGL loading = 5 wt%, TPPTS/Rh = 5 (molar ratio), substrate = 2 ml, toluene = 5 ml, T = 373 K, syngas (CO/H_2 = 1, volume ratio) = 2 MPa, reaction time = 4 h, agitation speed = 800 rpm.

[b] Reaction conditions: Rh(CO)$_2$(*acac*) = 0.0064 mmol, IL amount = 4.0 ml, others are the same as above.

Table 3
The hydroformylation of 1-hexene over several kinds of SILPCs[a]

Catalyst	IL loading (wt%)	Conversion (%)	n/i	TOF (h^{-1})	TOF per m^2 (h^{-1} m^{-2})
TPPTS-Rh/MCM-41	0	55.0	0.7	322	0.325
TMGL-TPPTS-Rh/MCM-41	5	55.6	2.7	348	0.606
	10	53.2	2.6	330	0.704
	15	56.5	3.0	389	0.968
	25	36.0	3.5	270	1.080
	50	27.9	2.5	197	1.288
TMGL-TPPTS-Rh/SiO_2	5	12.4	2.6	74	0.376
	10	16.1	2.6	106	0.914
	15	12.6	2.1	87	0.806
	25	9.1	2.0	68	0.829
	50	7.1	2.5	50	0.714
BMI·PF_6-TPPTS-Rh/MCM-41	5	50.2	1.8	298	0.478
	10	55.1	1.7	362	0.634
	15	48.5	1.7	334	0.677
	25	43.5	2.1	326	1.268
	50	35.2	1.8	249	1.025
BMI·BF_4-TPPTS-Rh/MCM-41	10	76.2	1.6	500	1.582

[a] Reaction conditions: Rh loading = 0.8 wt% (based on silicas) with the precursor Rh(CO)$_2$(*acac*), catalyst = 0.1 g, 1-hexene = 2 ml, toluene = 5 ml, syngas (CO/H_2 = 1, volume ratio) = 2 MPa, TPPTS/Rh = 5 (molar ratio), T = 373 K, reaction time = 4 h, agitation speed = 800 rpm.

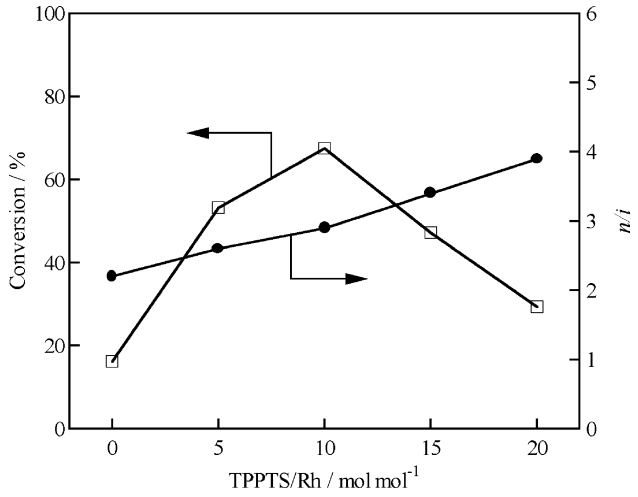

Fig. 8. The effect of TPPTS/Rh ratio on 1-hexene hydroformylation over the TMGL-TPPTS-Rh/MCM-41 SILPCs. Reaction conditions: TMGL loading = 10 wt%, others are the same as in Table 3.

decreases in the reaction rate and the n/i aldehyde ratio. The highest catalytic activity was obtained at a TMGL loading of 15 wt%, and the catalytic activity was almost independent of the type of IL. The results suggest that most of the catalytically active Rh complexes were dispersed in the ILs layers at the surface of MCM-41 in the case of proper IL loading, whereas a higher IL loading induced mass-transfer limitations.

Fig. 8 presents the 1-hexene conversion and n/i heptanal ratio as a function of the TPPTS/Rh molar ratio over the MCM-41-SILPC with 15 wt% TMGL. The n/i aldehyde ratio increased from 2.7 to 3.9, and the 1-hexene conversion decreased from 55.6 to 29%, when the molar ratio of TPPTS/Rh increased from 5 to 20. In the case of the monodentate TPPTS ligand system, rather low n/i aldehyde selectivities were obtained, as shown above. A higher n/i aldehyde selectivity might be obtained when a bidentate phosphine ligand is used [16].

Fig. 9 shows the results of the hydroformylation of 1-hexene over the various MCM-41-SILPCs as a function of the number of recycling runs. After the first reaction, the organic phase and the catalyst were separated by centrifugation, followed by decantation. The catalyst powder was directly reused for the next hydroformylation run. When TPPTS was used as a ligand, the SILPC with TMGL or BMI·PF_6 showed rather good stability. No dramatic fall in the catalytic activity was obtained at any time during the six experiments. The organic phase was colorless and the rhodium content was under the AAS detection level. In the case where PPh_3 was used as the ligand for the SILPC, however, although a better activity was obtained in the first run, the catalytic activity and selectivity showed significant losses in the successive recycling runs. The organic phase was yellowish in color, apparently because of the severe leaching of the rhodium species and PPh_3 ligand in the course of the reaction.

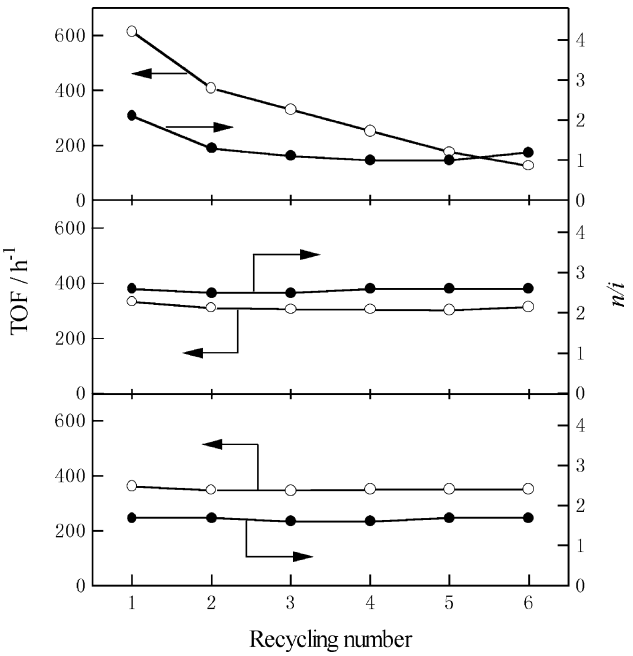

Fig. 9. The recycling results in 1-hexene hydroformylation over the MCM-41-SILPC. (a) TMGL-PPh_3-Rh/MCM-41; (b) TMGL-TPPTS-Rh/MCM-41; (c) BMI·PF_6-TPPTS-Rh/MCM-41. Reaction conditions are the same as in Fig. 8.

4. Conclusion

Immobilization of water-soluble TPPTS-Rh complex in the ILs TMGL, BMI·BF_4, and BMI·PF_6 on mesoporous MCM-41 silicas gave a better hydroformylation performance of 1-hexene than the corresponding IL-organic biphasic catalyst system and the one with SiO_2 as carrier. The catalytic performance of SILPC was almost independent of the type of IL. The combination of large surface area and uniform mesopore structure of MCM-41 was essential for the enhancement. Most probably, the active species *trans*-Rh(CO)(O–Si≡)$(TPPTS)_2$ was formed in the thin IL layer at the MCM-41 surface. The MCM-41-SILPC was stable and reusable for the olefin hydroformylation in the liquid phase. Because TMGL is halogen-free and is easily available, the MCM-41-SILPC derived is promising for the production of high-value fine chemicals.

Acknowledgments

The authors gratefully acknowledge financial support from the NSFC (20021002, 20473065 and 20433030) and the National Basic Research Priorities Programme (973-project) (G2000048008).

References

[1] J.S. Wilkes, Green Chem. 4 (2002) 73.
[2] J.L. Anthony, E.J. Maginn, J.F. Brennecke, J. Phys. Chem. B 106 (2002) 7315.
[3] S.T. Handy, Chem. Eur. J. 9 (2003) 2938.

[4] J.S. Wikes, J. Mol. Catal. A: Chem. 214 (2004) 11.
[5] K.R. Seddon, J. Chem. Tech. Biotechnol. 68 (1997) 351.
[6] T. Welton, Chem. Rev. 99 (1999) 2071.
[7] P.J. Dyson, D.J. Ellis, D.G. Parker, T. Welton, Chem. Commun. (1999) 25.
[8] P. Wasserscheid, W. Keim, Angew. Chem. Int. Ed. 39 (2000) 3772.
[9] R. Sheldon, Chem. Commun. (2001) 2399.
[10] C.M. Gordon, Appl. Catal. A: Gen. 222 (2001) 101.
[11] J. Dupont, R.F. de Souza, P.A.Z. Suarez, Chem. Rev. 102 (2002) 3667.
[12] D.B. Zhao, M. Wu, Y. Kou, E.Z. Min, Catal. Today 74 (2002) 157.
[13] H. Olivier-Bourbigou, L. Magna, J. Mol. Catal. A: Chem. 182/183 (2002) 419.
[14] P. Wasserscheid, T. Welton (Eds.), Ionic Liquids in Synthesis, Wiley–VCH, New York, 2003.
[15] C. Bauequin, J. Baudoux, J. Levillain, D. Cahard, A.-C. Gaumont, J.-C. Plaquevent, Tetrahedron: Asymm. 14 (2003) 3081.
[16] C.E. Song, Chem. Commun. (2004) 1033.
[17] W.P. Chen, L.J. Xu, C. Chatterton, J.L. Xiao, Chem. Commun. (1999) 1247.
[18] W. Keim, D. Vogt, H. Waffenschmidt, P. Wasserscheid, J. Catal. 186 (1999) 481.
[19] J. Dupont, S.M. Silva, R.F. de Souza, Catal. Lett. 77 (2001) 131.
[20] S.T. Handy, X.L. Zhang, Org. Lett. 3 (2001) 233.
[21] N. Audic, H. Clavier, M. Mauduit, J.-C. Guillemin, J. Am. Chem. Soc. 125 (2003) 9248.
[22] Y. Chauvin, L. Mussmann, H. Olivier, Angew. Chem., Int. Ed. 34 (1995) 2698.
[23] F. Favre, H. Olivier-Bourbigou, D. Commereue, L. Saussine, Chem. Commun. (2001) 1360.
[24] D. DeCastro, E. Sauvage, M.H. Valkenberg, W.F. Hölderich, J. Catal. 196 (2000) 86.
[25] C.P. Mehnert, R.A. Cook, N.C. Dispenziere, M.J. Afeworki, J. Am. Chem. Soc. 124 (2002) 12932.
[26] C.P. Mehnert, E.J. Mozeleski, R.A. Cook, Chem. Commun. (2002) 3010.
[27] A. Riisager, K.M. Eriksen, P. Wasserscheid, R. Fehrmann, Catal. Lett. 90 (2003) 149.
[28] A. Riisager, P. Wasserscheid, R. van Hal, R. Fehrmann, J. Catal. 219 (2003) 452.
[29] A. Wolfson, I.F.J. Vankelecom, P.A. Jacobs, Tetrahedron Lett. 44 (2003) 1195.
[30] H. Hagiwara, Y. Sugawara, K. Isobe, T. Hoshi, T. Suzuki, Org. Lett. 6 (2004) 2325.
[31] S. Breitenlechner, M. Fleck, T.E. Müller, A. Suppan, J. Mol. Catal. A: Chem. 214 (2004) 175.
[32] C.P. Mehnert, Chem. Eur. J. 11 (2004) 50.
[33] J. Huang, T. Jiang, H.X. Gao, B.X. Han, Z.M. Liu, W.Z. Wu, Y.H. Chang, G.Y. Zhao, Angew. Chem. Int. Ed. 43 (2004) 1397.
[34] A. Riisager, R. Fehrmann, S. Flicker, R. van Hal, M. Haumann, P. Wasserscheid, Angew. Chem. Int. Ed. 43 (2004) 2.
[35] J.S. Beck, J.C. Vartuli, W.J. Roth, M.E. Leonowicz, C.T. Kresge, K.D. Schmitt, C.T.W. Chu, D.H. Olson, E.W. Sheppard, S.B. McCullen, J.B. Higgins, J.L. Schlenker, J. Am. Chem. Soc. 114 (1992) 10834.
[36] A. Corma, Chem. Rev. 97 (1997) 2373.
[37] C.Y. Chen, H.X. Li, M.E. Davis, Micropor. Mater. 2 (1993) 17.
[38] J.M. Kim, J.H. Kwak, S. Jun, R. Ryoo, J. Phys. Chem. 99 (1995) 16742.
[39] R. Ryoo, S. Jun, J. Phys. Chem. B 101 (1997) 317.
[40] Y. Yang, H.Q. Lin, C.X. Deng, J.R. She, Y.Z. Yuan, Chem. Lett. 34 (2005) 220.
[41] Y.Z. Yuan, H.B. Zhang, Y.Q. Yang, Y. Zhang, K.R. Tsai, Catal. Today 74 (2002) 5.
[42] A.Z.Z. Paulo, E.I.D. Jeane, E. Sandra, Polyhedron 7 (1996) 1217.
[43] N.M.M. Mateus, L.C. Branco, N.M.T. Lourenco, C.A.M. Afonso, Green Chem. 3 (2003) 347.
[44] W. Cao, H.B. Zhang, Y.Z. Yuan, Catal. Lett. 91 (2003) 243.
[45] Q.R. Peng, Y. Yang, Y.Z. Yuan, J. Mol. Catal. A: Chem. 219 (2004) 175.
[46] Y.Z. Yuan, W. Cao, W.Z. Weng, J. Catal. 228 (2004) 311.
[47] S. Storck, H. Bretinger, W.F. Maier, Appl. Catal. A: Gen. 14 (1998) 137.
[48] J.D. Carruthers, P.A. Cutting, R.E. Day, M.R. Harris, S.A. Mitchell, K.S.W. Sing, Chem. Ind. 50 (1968) 1772.
[49] C.P. Mehnert, R.A. Cook, N.C. Dispenziere, E.J. Mozeleski, Polyhedron 23 (2004) 2679.
[50] F.R. Hartly, S.G. Murray, P.N. Nicholson, J. Mol. Catal. 16 (1982) 363.
[51] D.M. Barlex, M.J. Hacker, R.D.N. Kemmitt, J. Organomet. Chem. 43 (1972) 425.
[52] W.A. Hermann, J.A. Kulpe, W. Konkol, H. Bahrmann, J. Organomet. Chem. 389 (1992) 85.
[53] I.T. Horváth, Catal. Lett. 6 (1990) 43.